JOURNAL OF GEOPHYSICAL RESEARCH, VOL. 92, NO. D5, PAGES 5540–5554, MAY 20, 1987

An Investigation of Cloud/Radiation Interactions Using Three-Dimensional Nephanalysis and Earth Radiation Budget Data Bases

GEORGE KOENIG

Air Force Geophysics Laboratory, Hanscom Air Force Base, Bedford, Massachusetts

KUO-NAN LIOU AND MICHAEL GRIFFIN

Department of Meteorology, University of Utah, Salt Lake City

The cloud climatology data obtained from the analysis of the Air Force three-dimensional nephanalysis (3DNEPH) cloud data base and the broadband radiation budget data derived from the Nimbus 7 earth radiation budget (ERB) measurements, are compared on regional, zonally averaged, and hemispheric scales for January and July 1979. The analyzed cloud climatologies are also compared with existing cloud climatologies and general circulation features. In addition, they are used as input to an IR parameterization model to calculate the emitted IR flux at the top of the atmosphere. These model fluxes are subsequently compared with the ERB flux climatologies. An investigation of the sensitivity, at 1200 and 2400 local time, of the reflected solar, emitted IR, and net radiation to changes in cloud amount on a regional, zonal, and hemispherical basis is then carried out employing the 3DNEPH and ERB data. The daily net radiation sensitivity factors for the northern hemisphere for January and July, with values of -8.1 and -50.9 W m^{-2}, respectively, compare reasonably well with those obtained by other investigators.

1. INTRODUCTION

Clouds regularly occupy at least 50% of the sky on a global scale and are one of the most important regulators of the earth's radiation balance. Over a sufficiently long time the absorbed solar flux must be balanced by the outgoing terrestrial infrared flux. Globally and over a long time interval this balance seems to be maintained, but on a smaller scale in time and space this is not generally true. The temporary imbalances in the radiation budget result in differential heating of the globe, which, coupled with the rotation of the earth, drives the circulation of the atmosphere and the ocean currents. These circulations, in turn, regulate the distributions of temperature, cloudiness, and precipitation over the globe. An understanding of weather and climate, and the mechanisms of weather and climate changes, must begin with a detailed understanding of the radiative balance of the atmosphere and earth and of the factors, especially clouds, which influence that balance sufficiently to cause short- and long-term changes.

The presence of clouds greatly increases the solar radiation that is reflected back to space. This effect, known as the albedo effect, will reduce the solar radiation available to the earth-atmosphere system and will result in a cooling of this system. Clouds also reduce the thermal radiation emitted to space by absorbing long-wave radiation from the earth's surface, clouds, and the atmosphere below the cloud layer and by emitting long-wave radiation at normally colder cloud top temperatures. This effect, known as the greenhouse effect, increases the radiation budget, which, in general, results in a warming of the earth-atmosphere system. The net radiation available to the earth-atmosphere system, and thus the differential heating of the earth-atmosphere system, is strongly regulated by the horizontal extent, vertical position, thermodynamic phase, liquid/ice content, and particle size distributions of the clouds.

Paper number 7D0162.
0148-0227/87/007D-0162$05.00

On the basis of observed satellite data, *Cess* [1976], *Ohring and Clapp* [1980], *Hartmann and Short* [1980], *Ohring et al.* [1981], and *Cess et al.* [1982] examined the sensitivity of the net radiation budget of the earth-atmosphere system to variations in cloudiness. *Cess* [1976] determined that changes in either the zonal or global cloud amounts resulted in a corresponding change in the net radiation of approximately 2.6 W m^{-2}. This implies that on a zonal or global basis the albedo effect, as a result of changing cloud amounts, is balanced by the greenhouse effect. However, studies conducted by *Ohring and Clapp* [1980], *Hartmann and Short* [1980], and *Ohring et al.* [1981], using National Oceanic and Atmospheric Administration (NOAA) scanning radiometer data, indicated that the albedo effect is much greater than the greenhouse effect. In general, these studies have determined a net radiation sensitivity factor, defined as the change in the net radiation to changes in the cloud amount, ranging from -30 to -110 W m^{-2}, with a northern hemisphere average of -71 W m^{-2}.

It is evident from the aforementioned studies that on a regional basis, clouds represent an important radiative feedback mechanism. In fact, the low-latitude zone gradients of the net radiation sensitivity parameter can be as large as the meridional gradients. These studies indicate that the regional, day-to-day variability in the outgoing long-wave radiation is related to changes in the cloud amounts associated with the atmospheric circulation patterns. The disparity in the results of these studies clearly indicates the importance of establishing the cloud/radiation interactions.

However, the cloud/radiation interaction studies of *Cess* [1976], *Ohring et al.* [1981], and *Hartmann and Short* [1980] determine the net radiation and IR sensitivities to changes in the cloud amount from a knowledge of either the clear-sky and surface albedos or the planetary albedos. To date the values of these sensitivities have not been calculated using

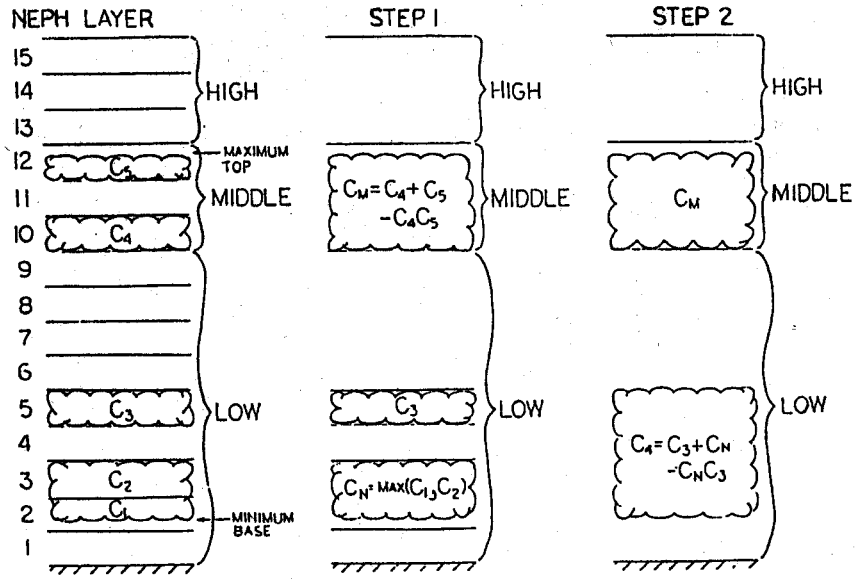

Fig. 1. Procedure used to combine 3DNEPH cloud layers to obtain the low, middle, and high cloud amounts.

actual cloud amounts. Moreover, the cloud/radiation studies of Ohring et al. and Hartmann and Short use earth radiation budget (ERB) data from satellites which measure the short-wave and long-wave radiances over a limited spectral interval. For example, the long-wave radiances are usually measured in the 10- to 12-μm infrared window. To obtain the total IR flux from these window measurements, it is necessary to apply some type of regression technique.

The prime objective of this paper is to utilize the cloud climatology data analyzed from the Air Force three-dimensional nephanalysis (3DNEPH) cloud data base and the broadband radiation budget data derived from the Nimbus 7 ERB measurements to compare the cloud climatology and ERB radiances on regional, zonally averaged, and hemispheric scales for January and July 1979. Section 2 of this paper describes the 3DNEPH cloud analysis and cloud climatology. In section 3, radiation budgets at the top of the atmosphere derived from the Nimbus 7 broadband radiances are presented. The resulting cloud/radiation comparison computed from these two data bases are subsequently discussed in section 4. Finally, conclusions are given in section 5.

2. Cloud Climatology Derived From 3DNEPH Data Base

The Air Force Global Weather Central (AFGWC) automated cloud analysis has been operational since early 1970. The model, also known as 3DNEPH, integrates satellite and conventional cloud information to produce a high-resolution global cloud analysis.

The horizontal resolution of the 3DNEPH is approximately 44 km at 60° latitude. The hemispherical grid consists of 262,144 grid points. To facilitate the computer processing, the hemispheric grid is divided into 64 (8 × 8) 3DNEPH boxes. Each 3DNEPH box contains 4096 (64 × 64) grid points.

The vertical grid consists of 15 layers of variable thickness which extend from the surface to about 17 km. The first six layers are above ground level (agl) layers, while the remaining layers are mean sea level (msl) layers. At grid points above sea level some of the msl layers may be partially or completely filled with terrain and/or agl layers. The valid time of the 3DNEPH analysis is 2400 UT, plus every 3 hours. The run time of the 3DNEPH is approximately 1 hour and 20 min after the valid time of the analysis. The delay in the running of the 3DNEPH ensures that a majority of the conventional reports within a valid time of the 3DNEPH are available for processing in the 3DNEPH analysis.

In the normal configuration, visual and infrared imagery data from the morning and noon sun-synchronous polar-orbiting Defense Meteorological Satellite Program (DMSP) satellites are used in the 3DNEPH analysis. The satellite data consist of visual and infrared daytime imagery and infrared nighttime imagery. The imagery from the DMSP satellite is preprocessed and stored in the Satellite Global Data Base (SGDB). The resolution of this data base is approximately 3 nm, which is equivalent to 64 (8 × 8) picture elements (pixels) per 3DNEPH grid point. The SGDB is continuously updated with new satellite imagery. The entire infrared data are updated approximately every 6–12 hours, while the entire visual data are updated every 18–24 hours. A threshold technique is used to process the satellite imagery to obtain the cloud information. This technique consists of comparing the satellite pixel information with the appropriate background information. The infrared satellite imagery is compared with a surface temperature field, while the visual imagery is compared with a dynamic background brightness field.

One of the major problems encountered with the 3DNEPH data base is the tremendous volume of data that must be processed to produce a cloud climatology. To reduce the data to a manageable size, the original 3DNEPH 15-layered cloud information is combined to produce a low, middle, high, and total (LMHT) cloud data base. A study conducted at AFGWC, based on surface observations for a 2-year period, indicated that more than three cloud layers were reported on less than 5% of the observations. In addition, the 3DNEPH grid points were averaged to convert from the high-resolution 3DNEPH grid system (44 km) to the ERB/subtarget area (STA) grid system (160 km).

The cloud information associated with the LMHT data

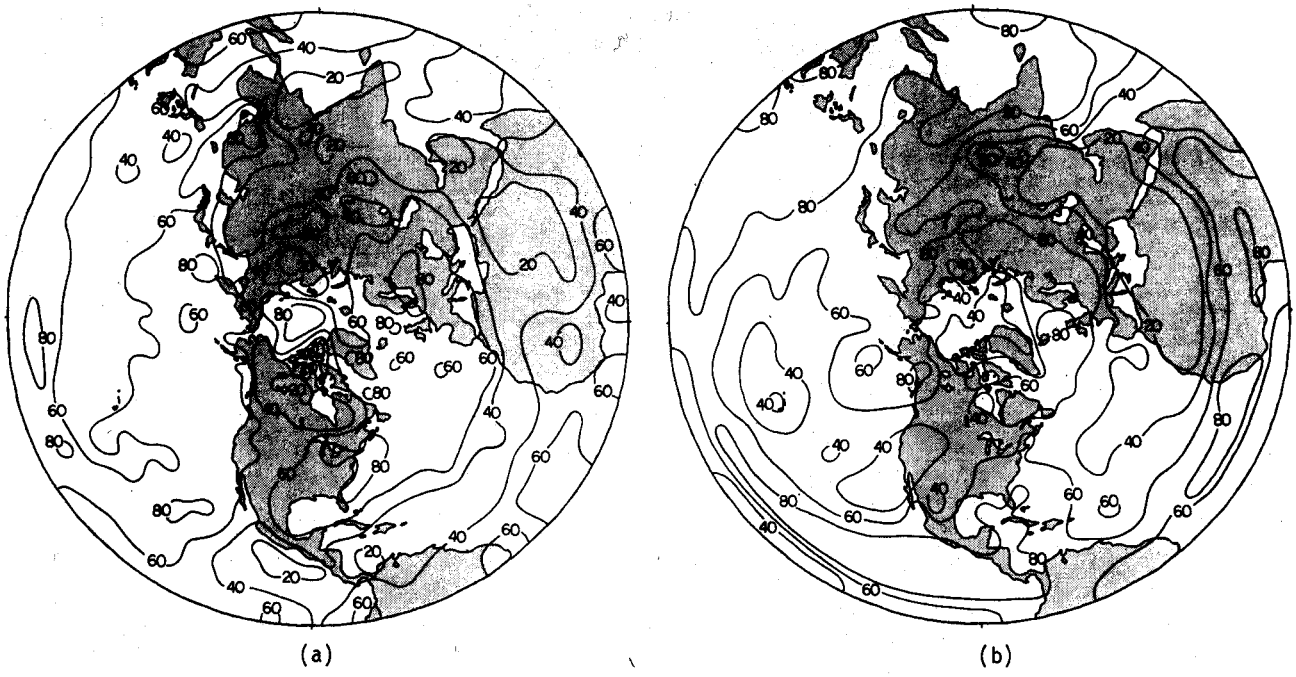

Fig. 2. The average daily (*a*) January and (*b*) July 3DNEPH total cloud amounts for the northern hemisphere.

base is obtained by combining specific 3DNEPH cloud layers. The 3DNEPH layers that are combined to generate the low, middle, and high (LMH) cloud amounts are a function of the grid point terrain height and the −20°C isotherm. The low/middle cloud boundary is defined as terrain height plus 2 km, while the middle/high cloud boundary is defined as terrain height plus height of the −20°C isotherm, which is a function of season and latitude. The grid point terrain heights were obtained from the AFGWC terrain/geography data base. This data base has the same horizontal resolution as the 3DNEPH data base. The height of the −20°C isotherm was determined from the atmospheric circulation statistics of *Oort and Rasmusson* [1971].

The LMH cloud amounts are obtained by using the principle of maximum overlap for contiguous 3DNEPH cloud layers and by using the principle of random overlap for noncontiguous 3DNEPH cloud layers. The following example illustrates the procedure used to determine the LMH cloud amounts. The lowest two 3DNEPH layers that contain clouds are combined, using either the principle of random or maximum overlap to produce a new layered cloud amount. This new layered cloud amount is then combined with the next highest 3DNEPH layer that contains clouds. This procedure is repeated until all of the 3DNEPH layers associated with a particular LMH cloud layer have been combined. For the example illustrated in Figure 1, the low cloud amount is calculated as follows.

First, we combine C_1 and C_2 using the principle of maximum overlap:

$$C_n = \max(C_1, C_2) \tag{1}$$

Assuming $C_1 > C_2$,

$$C_n = C_1 \tag{2}$$

Second, the low cloud amount is determined from the principle of random overlap in the form

$$C_l = C_n + C_3 - C_n(C_3) \tag{3}$$

The middle and high cloud amounts are determined in a similar manner.

The low, middle, and high cloud amounts are adjusted to be consistent with the 3DNEPH total cloud amount. The adjustment factor (AF) is based on the ratio of the 3DNEPH total cloud amount C_t and the calculated total cloud amount C_t', such that

$$\mathrm{AF} = C_t/C_t' \tag{4}$$

The calculated total cloud amount is based on the principle of random overlap and is determined from

$$\begin{aligned} C_t' &= 1 - (1 - C_l)(1 - C_m)(1 - C_h) \\ &= C_l + C_m + C_h - C_lC_m - C_lC_h - C_mC_h + C_lC_mC_h \end{aligned} \tag{5}$$

where C_l, C_m, and C_h are the low-, middle-, and high-layered cloud amounts, respectively. The low-, middle-, and high-layered cloud amounts are multiplied by the adjustment factor. This process is repeated until the calculated total cloud amount is within 2% of the observed total cloud amount (which usually occurs after the first iteration). The average AF, based on approximately 7×10^6 observations, is 0.98.

Most existing zonal cloud climatologies are presented in map form or as zonal averages, thus making it impossible to directly compare these climatologies with the 3DNEPH climatology. An alternate method, which can be used to determine the relative "goodness" of the 3DNEPH cloud climatology, is to compare the 3DNEPH cloud climatology to general circulation features and the ERB fluxes. The 3DNEPH cloud amounts should be consistent with the general circulation features and the ERB fluxes described in section 3. For the sake of brevity, only the average daily total cloud cover for January and July 1979 in the northern hemisphere will be presented here.

The most striking feature of the January 1979 cloud climatology (Figure 2*a*) is the almost continuous belt of low total cloud amounts associated with the subtropical high and the regions of high total cloud amounts south (Intertropical Convergence Zone (ITCZ)) and north (mid-latitude storm tracks) of the subtropical high. There is considerable longitudinal variation in the total cloud amounts in the equatorial regions. The cloud maxima along the east coast of the United States and China are associated with major storm tracks.

The most noticeable features of the July cloud climatology (Figure 2*b*) are the well-defined ITCZ in the Atlantic, western and eastern Pacific, and over equatorial Africa and the tropical and subtropical highs, located south and north of the ITCZ, in the Atlantic and eastern Pacific. In January a total cloud amount minimum is associated with the eastern Pacific off Central America. However, in July a total cloud maximum is associated with this region. The enhanced cloudiness in the north Atlantic and north Pacific, northern Europe, and northwestern U.S.S.R. is related to the mid-latitude storm tracks.

Figure 3 shows the zonal average daily low, middle, high, and total cloud climatology for January 1979. The maximum cloud amount in the vicinity of the equator correlates with the position of the ITCZ. The minimum total cloud amount north of this area is associated with the subtropical high. The maximum, extending from approximately 36° to 60°N is associated with the mid-latitude storm tracks. The maximum north of 72°N is most likely due to an error in the processing of the IR satellite information (visual satellite information does not exist for the polar latitudes in the wintertime hemisphere). If the IR satellite grey shades are incorrectly converted to a temperature and/or the surface/atmospheric temperature information is incorrect, it is possible that the land surfaces in the polar regions are being interpreted as clouds. The January 1977 zonal cloud climatology developed by *Gordon et al.* [1984], based on the 3DNEPH cloud information, also has extremely high total cloud amounts north of approximately 75°N.

The January tropical cloud maximum, associated with the ITCZ, moves approximately 10° northward in July and is better defined, as shown in Figure 4. In addition, the amplitude of the maximum increases significantly. The magnitude of this maximum is relatively high, but its presence is well documented by other cloud climatologies and the ERB data. In late June 1979 the satellite data from a new DMSP satellite was used operationally in the 3DNEPH analysis. Unfortunately, it takes 2 or 3 months to gather sufficient statistics to tune the visual and IR processors. The relatively low cloud amounts south and north of this maximum are associated with the tropical and subtropical high-pressure cells. In July the mid-latitude storm tracks move northward and are better defined. The shift in the position of the storm tracks is from approximately 35° to 50°N. Unlike the January zonal cloud analysis, the July analysis north of 75°N is usable.

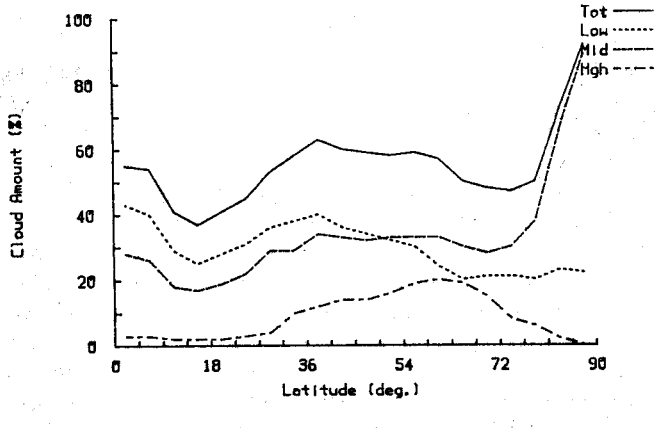

Fig. 3. Northern hemisphere average daily low, middle, high, and total zonal cloud climatology for January 1979.

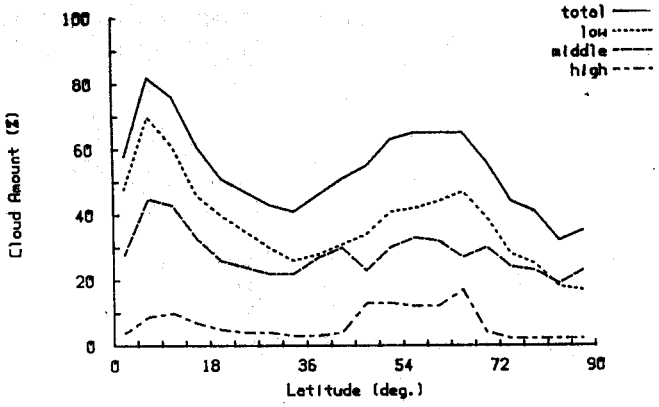

Fig. 4. Northern hemisphere average daily low, middle, high, and total zonal cloud climatology for July 1979.

Hughes [1984] presented the zonal averaged total cloud amounts for a number of climatologies. This information has been tabulated for five of the climatologies and is presented in Table 1. The results of the 3DNEPH zonal cloud climatologies for January and July are also listed in Table 1. All January cloud climatologies listed show enhanced total cloud amounts associated with the ITCZ (0°–10°N) and the mid-latitude storm tracks (20°–70°N). In addition, all cloud climatologies depict the region associated with the subtropical high (10°–20°N) as a region of relatively low total cloud amounts. The greatest difference between the 3DNEPH climatology and the average of the other climatologies (referred to as the average climatology) occurs for the 80°–90°N zonal belt. As mentioned earlier, the 3DNEPH analysis is not reliable for the polar regions of the wintertime hemisphere. The difference between the average climatology and the 3DNEPH climatology is less than half of the range given for the five climatologies for all latitude belts, except for the latitude belt from 80°–90°N. The average of the absolute difference between the average climatology and the 3DNEPH climatology is 8.1%.

The 3DNEPH July climatology differs considerably from the average climatology for the most southern latitude belt and the two most northern latitude belts. These latitude belts also exhibit considerable range between the five climatologies. As noted, the July cloud amounts in the tropics may be overestimated by the IR processor because of insufficient tuning factor statistics. The average of the absolute difference between the average climatology and the 3DNEPH climatology is 7.9%.

3. Radiation Budget Analyzed From ERB Data Base

One of the objectives of the ERB experiment aboard the Nimbus 7 satellite is to take broadband measurements of the angular radiance components of both the earth-reflected solar and earth-emitted IR radiation [*Jacobowitz et al.*, 1978]. These angular radiance components can be used to develop

TABLE 1. The 3DNEPH Zonal Total Cloud Climatology and Five Selected Total Cloud Climatologies for the Northern Hemisphere

Latitude	*Brooks* [1927]	*London* [1957]	*Schutz and Gates* [1971] *ETAC* [1971]	*Schutz and Gates* [1971] *Miller and Feddes* [1971]	*Berlyand and Strokina* [1980]	Range	Average	3DNEPH
				January				
90°–80°N	38	40	48	···	54	16	45	82
80°–70°N	56	47	49	···	59	12	53	48
70°–60°N	57	58	58	···	65	8	60	52
60°–50°N	59	63	66	49	69	20	61	58
50°–40°N	58	59	65	63	65	7	62	59
40°–30°N	50	51	58	50	59	9	54	58
30°–20°N	42	39	45	34	52	10	42	46
20°–10°N	40	36	···	18	48	30	35	40
10°–0°N	48	47	···	32	57	25	46	50
				July				
90°–80°N	86	64	83	94	84	30	82	34
80°–70°N	75	69	78	81	79	12	76	39
70°–60°N	68	66	69	56	72	16	66	55
60°–50°N	63	63	73	57	73	16	66	65
50°–40°N	51	55	62	50	61	11	55	56
40°–30°N	42	41	51	36	51	15	44	43
30°–20°N	45	42	49	38	51	9	45	47
20°–10°N	59	49	···	90	62	22	52	62
10°–0°N	56	54	···	44	64	20	54	72

This table is taken from *Hughes* [1984], except for the 3DNEPH results. ETAC stands for Environmental Technical Applications Center.

anisotropic factors for the reflected and emitted radiation as a function of the underlying surface (cloud versus the earth's surface) and the earth-satellite-sun geometry. With the aid of these models it is possible to determine the outgoing solar and IR fluxes at the top of the atmosphere with the narrow field of view (NFOV) radiance observations.

Nimbus 7 is a sun-synchronous polar-orbiting satellite with equator crossings at local noon (ascending) and midnight (descending). The NFOV instrument, which consists of eight channels, scans from nadir to the horizon in several vertical planes. Channels 15–18 measure the reflected solar radiation (0.2–4.8 μm), while channels 19–22 measure the emitted IR radiation (4.5–50 μm). The channels have a rectangular instantaneous field of view (IFOV) of 0.25° × 5.12°. Up to 20 IFOVs may be integrated to produce the desired field of view (FOV). The Nimbus 7 satellite is operated in five different scanning modes [*Jacobowitz et al.*, 1984]. These modes are designed to obtain a large number of angularly independent views of the same geographical area. The basic scan mode maintains a ground resolution that ranges from 90 × 90 km at nadir to approximately 250 × 250 km at the horizon. The scanning telescopes can sample 80% of the earth's viewable disc in just under 4 min. During this time, approximately 1700 radiance observations are recorded.

The NFOV radiance observations from Nimbus 7 are sorted into 2070 target areas (TA) covering the entire globe. Each TA is approximately 500 × 500 km. The TAs are subdivided into 3 × 3 subtarget areas, with a resolution of 160 × 160 km. The radiance values associated with each STA are sorted into angular bins based on time and viewing geometry. The viewing geometry is defined by the satellite zenith angle θ and relative (to the sun) satellite azimuth angle ϕ. The STA radiance information forms the basic data set of the subtarget radiance tape (STRT).

The STRT consists of three records: topography, geography, and orbital. The orbital record is subdivided into cloud and radiance observation subrecords. The topography record for each TA gives a description of the earth's surface characteristics and the vegetation types associated with the TA. The geography record for each STA gives the percent of the STA that is land, water, snow, and ice, respectively. The cloud orbital record contains sky/cloud conditions for clear, low, middle, and high clouds for each orbital sighting of a STA. The sky/cloud information is based on temperature-humidity infrared radiometer (THIR) measurements.

To convert an observed radiance value to an equivalent flux value it is normally necessary to apply both a geometrical and spectral transformation. Since the Nimbus 7 NFOV sensors cover a broad spectrum (0.2–4.8 μm shortwave and 4.5–50 μm long wave) it is not necessary to employ a spectral transformation when converting radiance measurements to flux measurements. *Taylor et al.* [1983*a*, *b*] have developed anisotropic emission factors (AEF) and anisotropic reflectance factors (ARF) based on 270 days of uniformly distributed Nimbus 7 radiance observations for the period from November 1978 to May 1980. These factors are defined as the ratio between an actual radiance and a radiance that would be observed if the same energy were emitted (reflected) isotropically. Using the anisotropic factors from the NASA archive, the outgoing IR radiance value $R(\theta')$ associated with a specific STA is converted to a flux value by multiplying by a correction factor π/AEF, which is a function of season, latitude, satellite zenith angle, and the underlying suface. In a similar fashion, a reflected solar radiance value $R(\theta', \phi')$ can be converted to a flux value via a correction factor π/ARF, which has an additional dependence on the solar zenith angle and the relative azimuthal angle between the sun and satellite. Because of the instability of the anisotropic factors at the large satellite zenith

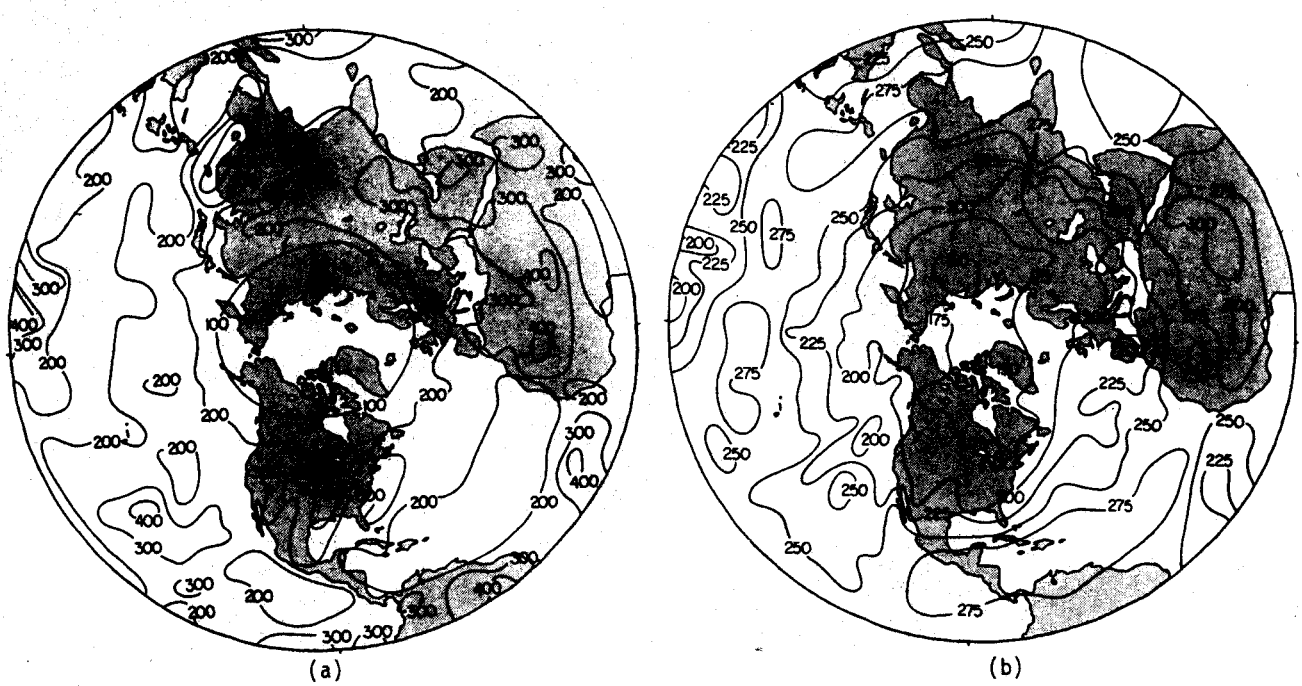

Fig. 5. Nimbus 7 ERB 1200 LT (*a*) reflected solar and (*b*) outgoing IR fluxes for the northern hemisphere for January 1979. Units are in watts per square meter.

angles, observations at angles greater than 50° were not included in the analysis.

Figure 5*a* depicts the 1200 LT reflected solar flux and Figure 5*b* the emitted IR flux values for January 1979. Over the oceanic and subtropical high regions the solar flux is out of phase with the emitted IR flux. In these regions the outgoing IR flux is relatively high, while the reflected solar flux is low. Over the Afro-Asian desert, both the outgoing solar and IF flux values are high. The outgoing IR flux shows both a maximum and a minimum over the tropical eastern Pacific (115°–140°W and 10°–20°N) associated with the cloud configuration depicted in Figure 2*a*. A maximum in the solar flux, and hence the albedo, coincides with the maximum in the outgoing IR flux. These maxima are associated with stratus cloud fields which have relatively warm cloud top temperatures, while the IR flux minimum is associated with clouds with colder cloud top temperatures.

The equatorial regions of high reflected solar flux and low outgoing IR flux are correlated with a higher total cloud amount. The strong outgoing IR flux gradients, associated with the outgoing IR flux minima in the central and western Pacific and east central Atlantic, imply large spatial variations in the surface–cloud top temperature difference. These large variations are characteristic of an area with considerable convective activity. The reflected solar and outgoing IR flux values are relatively high along the east coast of the United States and China. The influence of the high total cloud amounts associated with these regions on the outgoing IR flux is not very evident, especially over eastern China. Regions of uniform outgoing IR flux imply that the cloud top temperatures are fairly uniform. The low outgoing IR flux, high reflected solar flux and albedos, and relatively clear skies associated with the Rockies reflect the influence of cold, snow-covered mountains. The high reflected solar flux values for the Mississippi Valley are most likely associated with the Gulf Coast stratus found in this region during the winter. The strong meridional gradients of surface temperature and incoming solar radiation for the northern latitudes are very evident on the maps of the outgoing IR and solar fluxes.

On the July map illustrated in Figure 6, low outgoing IR flux values are associated with the ITCZ, high values over the Afro-Asian desert, low albedos and solar flux values over the tropical and subtropical oceanic highs, and high values over the deserts. The eastern Pacific off Central America is also a region of low outgoing IR flux values in July, indicating considerable convective activity. The stratus cloud fields off the west coast of the United States are defined by high outgoing long-wave and shortwave flux values. The outgoing IR flux values are high because the surface–cloud top temperature difference is small. The monsoon, which extends from India through central and eastern China to Korea and Japan, is characterized by high reflected solar flux values and low outgoing IR flux values. The mid-latitude storm tracks move northward in July and are not as well defined. The solar fluxes, and hence the high albedos over Greenland, are associated with the ice cap.

Figure 7 depicts the variations with latitude of the outgoing IR flux and solar fluxes and the daily average albedo for January 1979. The daily average albedo is defined as the ratio of the daily average reflected solar flux to the incoming daily solar insolation. To obtain the daily average reflected solar flux, a correction for the change in solar zenith angle and underlying surface with time must be applied to the instantaneous reflected solar flux. *Taylor and Stowe* [1984] computed values for the change in albedo with solar zenith angle for each of four underlying surface types and four cloud types. The surface types (land, ocean, snow, or ice) were obtained from the ERB geographical record, while the cloud types (low, middle, high, and total) were derived from THIR data and are included in the orbital record. These values were incorporated

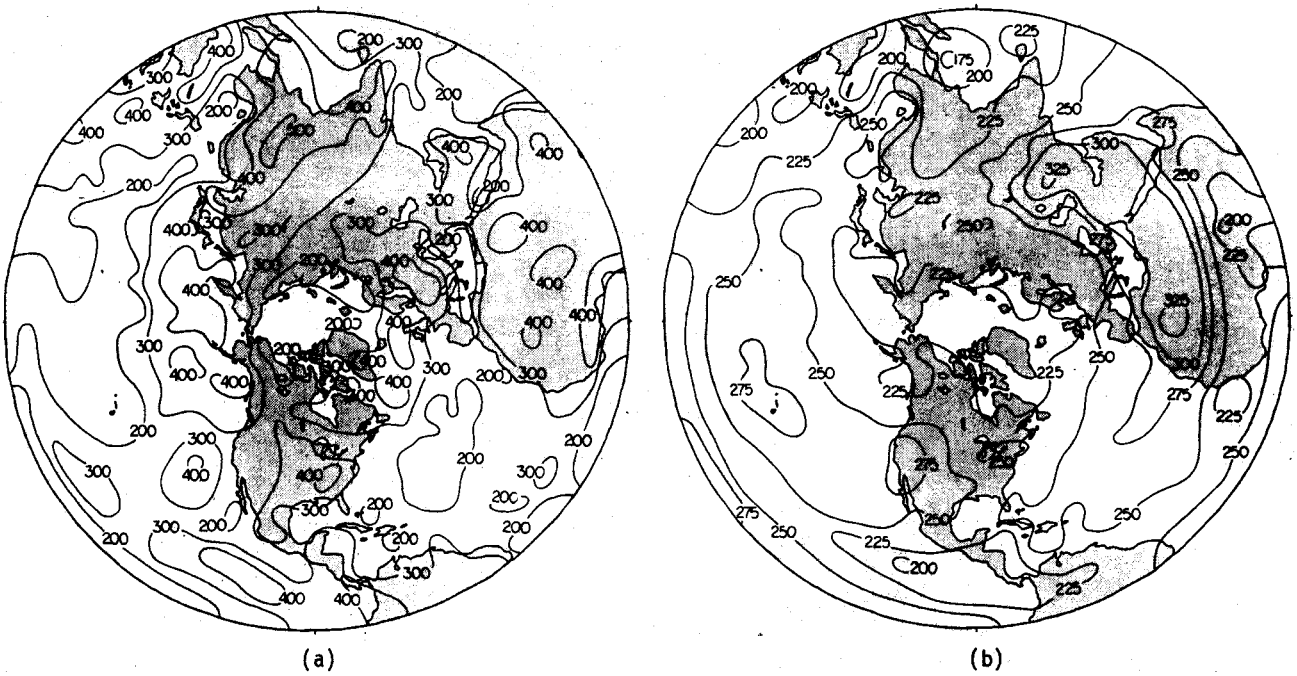

Fig. 6. Nimbus 7 ERB 1200 LT (*a*) reflected solar and (*b*) outgoing IR fluxes for the northern hemisphere for July 1979. Units are in watts per square meter.

into a model that computed a modified correction factor as a function of solar zenith angle by weighting them with the fraction of the STA covered by the corresponding surface. Following the method of *Jacobowitz et al.* [1984], these factors were used to produce a daily average conversion factor which could be applied to the instantaneous flux values. It is noted that the manner in which the correction factors and averaging method are applied to the instantaneous radiance data has a nonnegligible effect on the derived albedo [*Arking and Vemury*, 1984]. The variations in the outgoing fluxes correlate with the variations in the total cloud amounts equatorward of 50°N. The minimum in the outgoing solar flux and albedo and the maximum in the outgoing IR flux, in the region from 10° to 22°N, reflects the decrease in the total cloud amounts associated with the subtropical high. The sharp decrease in the outgoing solar flux north of 45°N is due mainly to the earth-sun-satellite geometry. In fact, the albedo actually increases in this region. In addition, for the northern latitudes, part of the increase in the albedo is due to an increase in the aerial extent of the snow/ice cover. Poleward of 25°N the outgoing IR flux steadily decreases. In part this decrease is due to the decrease in the surface and atmospheric temperatures.

In July 1979, shown in Figure 8, the solar and IR flux variations correlate with the total cloud variations south of 70°N. The two well-defined shortwave maxima are associated with the ITCZ and mid-latitude storm tracks. The outgoing IR flux decreases in these regions, with the largest decrease associated with the ITCZ. This relatively large decrease in the outgoing IR flux implies that the cloud top–surface temperature difference is relatively large. North of 70°N the outgoing solar flux increases rapidly in response to the earth-sun-satellite geometry effects and an increase in snow/ice coverage.

Finally, we compare the computed IR flux at the top of the atmosphere with the observed IR flux, using the corresponding 3DNEPH layered cloud data described in section 2. The IR radiative transfer scheme employed is based on that developed at the University of Utah over a number of years [*Liou and Wittman*, 1979; *Liou and Ou*, 1981; *Ou and Liou*, 1983]. The model parameterization of the IR flux is based on the individual broadband emissivities for the H_2O rotational band, H_2O vibrational-rotational band, H_2O continuum, CO_2 and O_3 bands, and a correction for the H_2O–CO_2 overlap. The components contributing to the total emitted IR flux at the top of the atmosphere are the emitted surface, cloud, and atmospheric IR flux, attenuated by the intervening atmosphere and nonblack clouds, and the emitted atmospheric IR flux that is reflected upward by nonblack clouds. This reflected component will be attenuated by the atmosphere between the top of the reflecting cloud and the top of the atmosphere. It has been assumed that the low and middle clouds are black

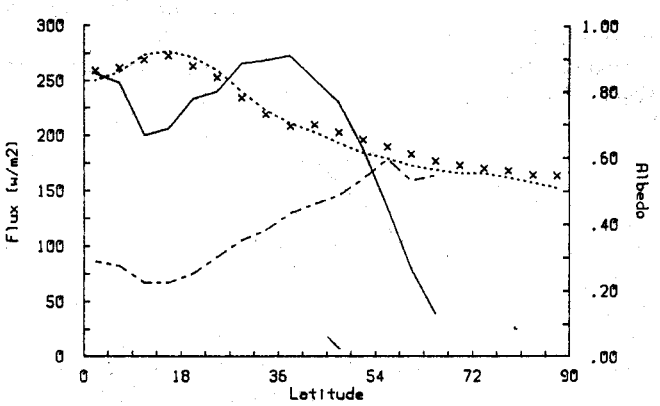

Fig. 7. Northern hemisphere outgoing IR flux at the top of the atmosphere: observed (dashed line), computed (crosses); 1200 LT reflected solar flux at the top of the atmosphere (solid line); and average daily albedo (long and short dash line) for January 1979.

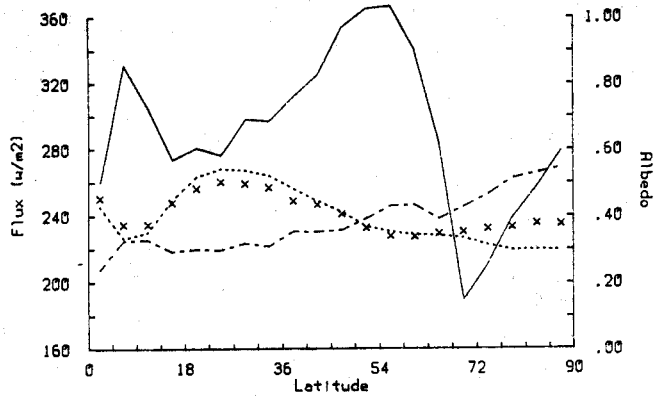

Fig. 8. Northern hemisphere outgoing IR flux at the top of the atmosphere: observed (dashed line); computed (crosses); 1200 LT reflected solar flux at the top of the atmosphere (solid line); and average daily albedo (long and short dash line) for July 1979. (Note that the y axis ranges from 160 to 360 W m^{-2}).

and the high clouds are nonblack. The emissivity, reflectivity, and transmissivity are calculated using the parameterization, developed by *Liou and Wittman* [1979], of the cloud radiative properties as a function of the ice water path, which is a function of ice water content and the cloud thickness. The ice water content has been parameterized as a function of temperature based on the data of *Heymsfield and Platt* [1984].

The contribution of each flux component to the total upward flux at the top of the atmosphere is a function of the geometrical cloud configuration. For three cloud layers there are seven geometrical cloud configurations. Using the principle of random overlap and the appropriate cloud layer amount, the IR fluxes are calculated.

This model is used with the 3DNEPH layered cloud climatologies and the atmospheric circulation statistics of *Oort and Rasmusson* [1971] to generate the outgoing IR flux at the top of the atmosphere. The computed IR fluxes for January and July are depicted in Figures 7 and 8, respectively. For the January case the average of the absolute difference is 7.0 W m^{-2}, while it is 6.3 W m^{-2} for July. It was found that the surface temperatures and cloud top heights are the most significant factors affecting the computed IR fluxes at the top of the atmosphere.

4. CLOUD/RADIATION INTERACTIONS

The 3DNEPH cloud and ERB reflected solar and emitted IR flux climatologies at 1200 LT can be used to calculate a number of cloud/radiation sensitivity factors. Let the total cloud cover, reflected solar flux, emitted IR flux, and net flux at the top of the atmosphere be denoted by η, F_S, F_{IR}, and F_N, respectively. Since clouds have a dominant effect on the radiation field of the earth-atmosphere system, we may then correlate the solar and IR fluxes with the total cloud amount in the forms

$$F_S = a_1 + b_1\eta \tag{6}$$

$$F_{IR} = a_2 + b_2\eta \tag{7}$$

where the slopes $b_1 = \Delta F_S/\Delta\eta$ and $b_2 = \Delta F_{IR}/\Delta\eta$ may be calculated from the least squares linear regression line of either F_S or F_{IR} versus η at each grid point. The net radiation sensitivity is then calculated from

$$\Delta F_N/\Delta\eta = -\Delta F_S/\Delta\eta - \Delta F_{IR}/\Delta\eta \tag{8}$$

4.1. *Regional Results*

To investigate the cloud/radiation sensitivity factors on a regional basis, scatter diagrams of the 1200 LT $F_{IR} - \eta$ and $F_S - \eta$ are plotted for selected STAs for January and July 1979. The regions selected either coincide with the regions used by *Hartmann and Short* [1980] or homogeneous climate zones [*Müller*, 1982]. The data used by Hartmann and Short were for a 3-month period, while the data used in this research were for a single month. In our analysis each region consists of approximately 90 STAs. The scatter diagrams of $F_{IR} - \eta$, $F_S - \eta$, and $F_{IR} - r$ (albedo at 1200 LT) are used to determine $\Delta F_{IR}/\Delta\eta$, $\Delta F_S/\Delta\eta$, and $\Delta F_{IR}/\Delta r$, respectively. In general, the outgoing flux is a function of noncloud-related variables (surface temperature, surface albedo, atmospheric temperature, and water vapor densities, etc.) and cloud-related variables (cloud amount, cloud top temperature, and cloud optical properties). It is assumed that the sensitivity of the outgoing flux to changes in noncloud-related variables is small compared to the sensitivity of the outgoing flux to changes in cloud-related variables. The temporal variations in the noncloud-related variables have been minimized by using cloud and ERB data at the same local time (1200 LT) each day. In addition, the spatial variations in the noncloud-related variables have been minimized by selecting areas that are climatologically homogeneous. Therefore it appears reasonable to assume that the slope of the linear regression line relates the change in the outgoing flux to the change in the cloud-related variables.

For the January case, four regions were selected for the analysis, and the results are listed in Table 2*a*. The scatter diagrams of the solar and IR fluxes versus cloud amount for these regions are shown in Figure 9. $\Delta F_{IR}/\Delta r$ is calculated from the 1200 LT scatter diagrams of $F_{IR} - r$. The scatter diagrams of $F_{IR} - r$ have not been presented here, but they can be found in the work by *Koenig* [1985]. Eastern China (region 1; 22°–30°N, 105°–115°E) is an area of persistent stratus during the winter. This area is characterized by maximum cloud amounts, albedo, and reflected solar fluxes. Since the cloud top–surface temperature difference is small, the outgoing IR flux is not very sensitive to changes in the low cloud amount. In fact, $\Delta F_{IR}/\Delta\eta$ is only -13.2 W m^{-2}. The small scatter of the points about the F_{IR} linear regression line indicates very little variation in the surface–cloud top temperature difference. The 1200 LT value of $\Delta F_N/\Delta\eta$ is -99.02, indicating that the albedo effect is greater than the greenhouse effect. The relatively large scatter of points associated with the plot of the

TABLE 2*a*. Radiation Sensitivity Factors for January

Region	$\Delta F_S/\Delta\eta$	$\Delta F_{IR}/\Delta\eta$	$\Delta F_N/\Delta\eta$	$\Delta F_{IR}/\Delta r$	$\Delta F_{IR}/\Delta r$ (Hartman and Short)
1	112.22	−13.20	−99.02	−73.81	−32.2
2	162.45	−45.02	−117.4	−125.63	−185.2
3	20.27	−45.69	25.42	29.79	37.0
4	87.99	−48.68	−39.31	−270.48	−250.0

Region 1, eastern China; 2, mid-latitude storm track; 3, western Russia; 4, Saharan Desert.

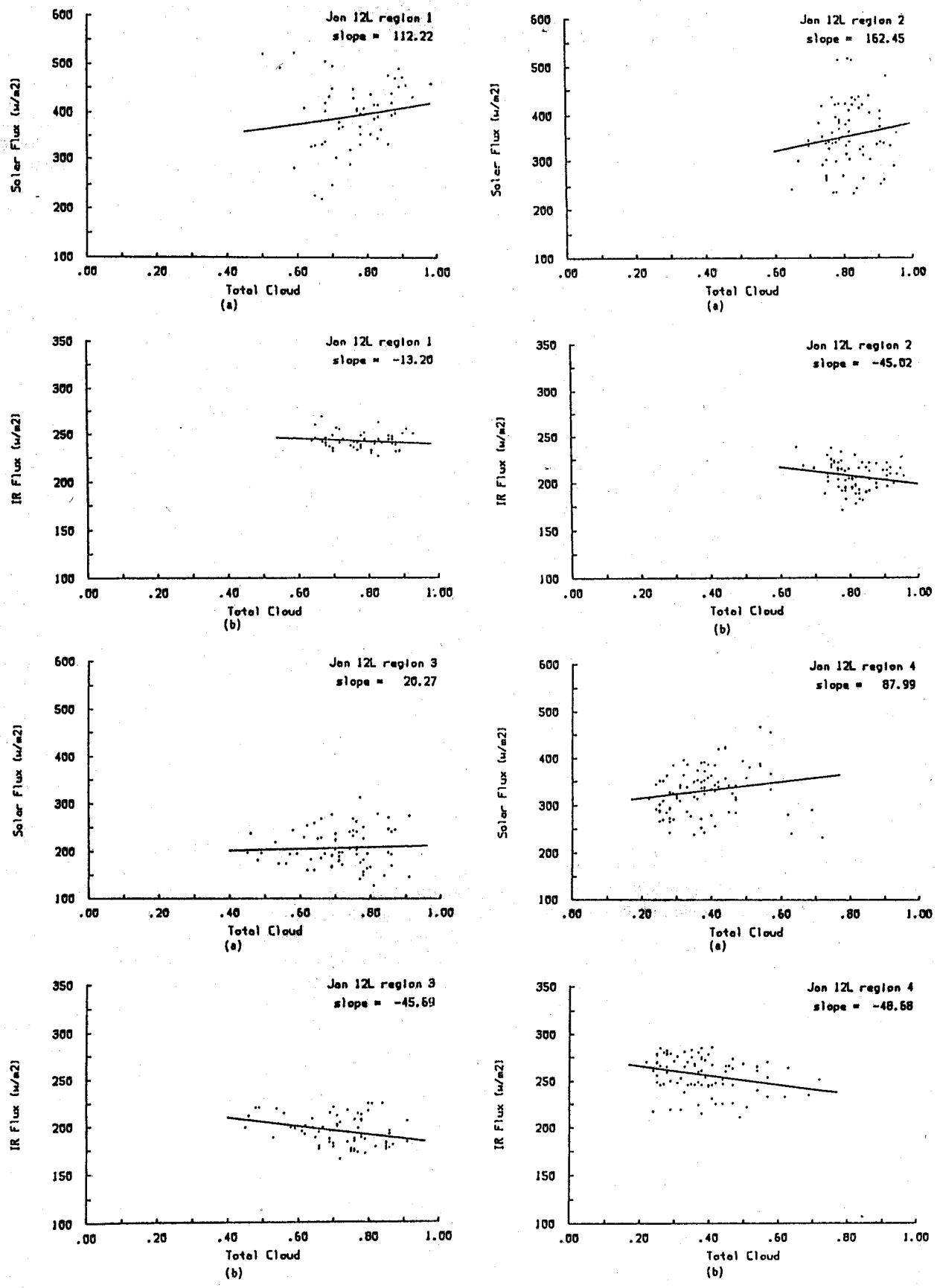

Fig. 9. Scatter diagrams for January of (*a*) 1200 LT reflected solar flux versus total cloud amount and (*b*) the 1200 LT outgoing IR flux versus total cloud amount for regions 1, eastern China; 2, mid-latitude storm track; 3, western Russia; and 4, Saharan desert. The solid line represents a least squares fit to approximately 90 data points.

solar flux is due, in part, to variations of the sun-earth-satellite geometry. The 1200 LT $\Delta F_{IR}/\Delta r$ sensitivity factor is -73.81 W m^{-3}, while the value calculated by Hartmann and Short is -32.2 W m^{-2}. The ranges of both the outgoing IR flux and the albedo for the two studies are similar.

Region 2 (31°–45°N, with a longitudinal width of approximately 10°), associated with the mid-latitude storm track, is located off the east coast of the United States and is characterized by both convective and stratiform clouds. Both the IR and solar flux sensitivities and the scatter of outgoing IR points about the linear regression line are greater than those of region 1. The increase in the scatter of the IR points is characteristic of an area with variable cloud top temperatures. The 1200 LT value of $\Delta F_N/\Delta\eta$ is -117.4, indicating that the albedo effect is greater than the greenhouse effect.

Region 3 (western Russia; 49°–63°N, 32°–64°E) is very interesting. The IR sensitivity factor is very similar to that of region 2, but the solar sensitivity factor is considerably different. As the cloud amount decreases, the reflected solar flux decreases only slightly, indicating high surface albedos. These high surface albedos are most likely due to extensive snow cover. Since the solar sensitivity factor is small, the net radiation factor is positive (25.42 W m^{-2}), and the greenhouse effect is greater than the albedo effect. An increase in the cloud amount increases the net radiation available to the earth-atmosphere system. Thus clouds "trap" more outgoing IR radiation than they reflect incoming solar radiation. The value of $\Delta F_{IR}/\Delta r$, calculated by Hartmann and Short, is consistent with the value of the net radiation sensitivity factor indicated earlier.

Region 4 (18°–31°N, 10°W to 10°E) is the Saharan desert. Even though the albedo effect is greater than the greenhouse effect, the net radiation is fairly sensitive to changes in the cloud amount. Because of the high surface albedo, the solar sensitivity factor is small. For example, the 1200 LT solar sensitivity factor for this region is 87.99 W m^{-2}, while the factor for region 2 is 162.45 W m^{-2}. The IR/albedo sensitivity is very large, indicating considerable surface–cloud top temperature difference. Hartmann and Short also calculated a large negative IR/albedo sensitivity factor for this region.

For the July case, four regions were chosen for the sensitivity analysis. The results are presented in Table 2*b* and Figure 10.

Region 1 (western Pacific ITCZ; 0°–13°N, 135°–148°W) is an ocean region of high total cloud amounts and considerable convective activity and large solar and IR sensitivity factors. In part this is due to the relatively high 3DNEPH cloud amounts in the tropics during July. In tropical ocean regions the variability of the surface and atmospheric temperature and atmospheric moisture is fairly small. Therefore the scatter in the outgoing IR plot is due mainly to cloud top temperature differences. The value of the net radiation sensitivity factor is unrealistically high. An increase in the convective cloud amount for ocean regions results in a significant increase in the reflected solar flux and a significant decrease in the outgoing IR flux. Therefore the net radiation factor should be small, while the IR/albedo sensitivity factor should be large. The IR/albedo value for this region is large, but the net radiation sensitivity value is also large, indicating a possible error in the cloud analysis. For most regions a comparison of the sensitivity factors can be used qualitatively to verify the cloud climatology. In addition, information concerning the cloud characteristics can be obtained from these sensitivity factors. For example, over stratus fields the net radiation sensitivity value will be large, while the IR/albedo sensitivity will be small, which is consistent with the warm uniform cloud tops associated with stratus.

Region 2 (27°–40°N, 120°–137°W) is associated with California stratus. The sensitivity factors are characteristic of a region where the surface–cloud top temperature differences are small. Both the solar and net radiation sensitivity factors are large, while the IR and IR/albedo sensitivity factors are small. Because of the relatively large sensitivity of the net radiation to changes in the cloud amount, these regions are important in climate studies.

In region 3 (eastern Russia; 58°–70°N, 110°–140°E) the value of $\Delta F_{IR}/\Delta r$ differs considerably from the value obtained by Hartmann and Short. The data used by Hartmann and Short were for a 3-month period (June, July, and August), while the data used in this research are for only a single month. Considerable cloud type variability over the longer period could result in larger $\Delta F_{IR}/\Delta r$ sensitivity factors. From the values of the sensitivity factors associated with this research, it appears that the predominant cloud type for this region during July is stratus.

It is evident from the values of the sensitivity factors that the predominant cloud type associated with region 4 (Norwegian sea; 48°–70°N, 10°W to 10°E) is stratus. The value of the IR/albedo sensitivity factor is consistent with the IR/albedo sensitivity factor obtained by Hartmann and Short.

4.2. *Zonally Averaged Results*

The solar, infrared, and net radiation sensitivity factors are calculated for each TA based on the day-to-day 1200 LT changes in the solar and IR fluxes and the changes in the total cloud amount. This information is used to compute the monthly zonal averages of the 1200 LT sensitivity factors. In general, the zonally averaged sensitivity factors reflect the general circulation features. The largest values of the IR and solar sensitivity factors are associated with the ITCZ and the mid-latitude storm tracks. The sensitivity factors associated with the tropical and subtropical highs and the polar regions are relatively small. In addition, the sensitivity factors decrease rapidly north of 40° and 60°N in January and July, respectively (Tables 3*a* and 3*b*). The strong gradients of the sensitivity factors for the northern latitudes reflect the influence of the meridional gradients of surface temperature and incoming solar radiation. The IR sensitivity factors have not been calculated north of 65°N for January because of the unreliable cloud climatology for this area.

TABLE 2*b*. Radiation Sensitivity Factors for July.

Region	$\Delta F_S/\Delta\eta$	$\Delta F_{IR}/\Delta\eta$	$\Delta F_N/\Delta\eta$	$\Delta F_{IR}/\Delta r$	$\Delta F_{IR}/\Delta r$ (Hartman and Short)
1	367.09	−93.54	−273.55	−326.09	−217.0
2	115.42	−48.71	−66.71	−6.0	−25.0
3	288.35	−22.70	−256.60	−52.54	−172.0
4	560.75	−38.11	−522.60	−42.94	−37.2

Region 1, western Pacific ITCZ; 2, California stratus; 3, eastern Pacific; 4, Norwegian sea.

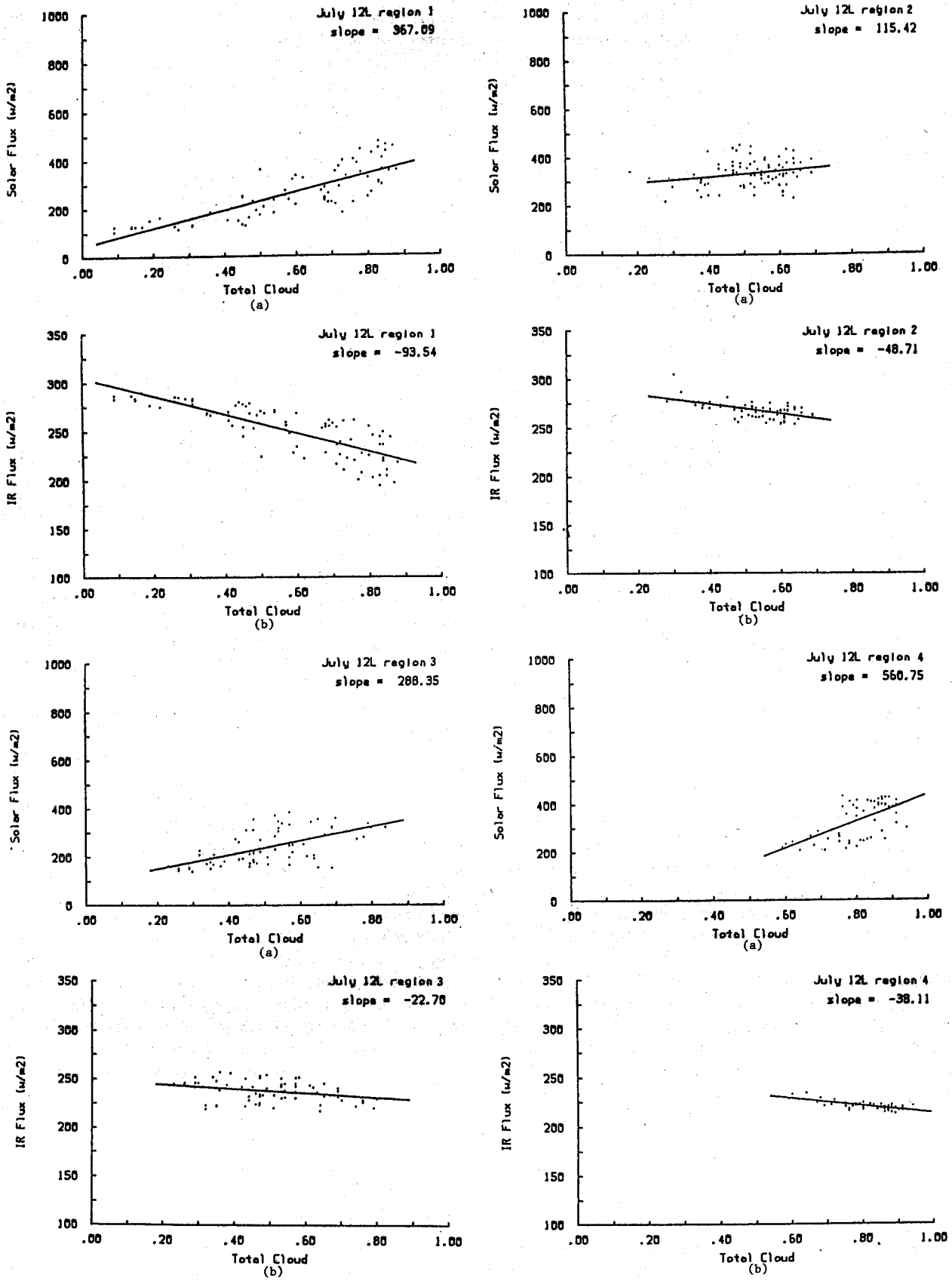

Fig. 10. Scatter diagrams for July of (*a*) the 1200 LT reflected solar flux versus total cloud amount and (*b*) the 1200 LT outgoing IR flux versus total cloud amount for regions 1, west Pacific ITCZ; 2, California stratus; 3, eastern Russia; and 4, Norwegian sea. The solid line represents a least squares fit to approximately 90 data points.

The greenhouse effect is greater than the albedo effect north of 60°N for January. Northward of approximately 75°N, during January the solar sensitivity factor will be zero and the net radiation sensitivity factor will be the negative of the IR sensitivity factor. Since the IR sensitivity factor is usually negative, the net radiation sensitivity will be positive. In July the net radiation is only positive for the most northern latitude belt. In general, the sensitivity values are greater in July.

Finally, the average daily net radiation sensitivity factors are calculated using the average daily solar and IR sensitivity factors in the form

$$\Delta\overline{F_N}/\Delta\bar{\eta} = -\Delta\overline{F_S}/\Delta\bar{\eta} - \Delta\overline{F_{IR}}/\Delta\bar{\eta} \quad (9)$$

where the overbars denote the average daily values. The average daily reflected solar flux is derived by applying a directional correction factor [*Taylor and Stowe*, 1984] and fractional sunlight hour mentioned previously. The average daily IR flux is obtained by averaging the 1200 and 2400 LT IR fluxes, weighted, by the number of hours of daylight and darkness, respectively. The results are depicted in the far right-hand columns of Tables 3*a* and 3*b*. The average daily net radiation sensitivity factors are less than the 1200 LT values, which is especially evident in the tropics and middle latitudes. The northern hemisphere average daily net radiation sensitivity factors are −8.1 and −50.9 W m^{-2} for January and July conditions, respectively. These values compare reasonably well with those determined by other investigators. For example, *Ohring et al.* [1981] calculated an annual northern hemisphere (0°–60°N) net radiation sensitivity factor of −71 W m^{-2}, *Hartmann and Short* [1980] gave the annual global net radiation sensitivity factor as −35 to −100W m^{-2}, and *Schneider* [1972] computed an annual global value of −58 W m^{-2}.

TABLE 3*a*. The Zonal Solar ($\Delta F_S/\Delta\eta$), IR ($\Delta F_{IR}/\Delta\eta$), and Net ($\delta F_N/\Delta\eta$) Sensitivity Factors for January

Latitude	Solar (1200 LT)	IR (1200 LT)	Net (1200 LT)	Net (Average Daily)
2.25	243.2	−68.7	−174.5	−32.8
6.75	292.7	−80.8	−211.9	−32.7
11.25	221.6	−67.6	−154.0	−16.3
15.75	188.4	−64.1	−124.3	−6.2
20.25	204.4	−67.2	−137.2	−2.0
24.75	261.2	−74.9	−186.3	−13.4
29.25	271.0	−76.6	−194.4	−10.6
33.75	263.2	−74.0	−189.2	−6.8
38.25	201.7	−68.5	−133.3	6.9
42.75	187.1	−52.3	−134.9	−0.4
47.25	108.6	−37.3	−71.3	6.7
51.75	74.0	−19.6	−54.3	0.0
56.25	54.6	−23.6	−31.0	6.5
60.75	22.8	−14.9	−7.9	8.3
65.25	0.9	−9.1	8.2	8.1
69.75	0.0	...	...	...
74.25	0.0	...	...	...
78.75	0.0	...	...	...
83.25	0.0	...	...	...
87.75	0.0	...	...	...
Northern hemisphere (0°–68°N)	191.9	−57.5	−134.4	−8.1

Sensitivity factors are stated in units of watts per square meter/percent. IR sensitivity factors north of 65°N were not calculated for January because of the potential inaccuracies of the cloud climatology.

TABLE 3*b*. The Zonal Solar ($\Delta F_S/\Delta\eta$), IR ($\Delta F_{IR}/\Delta\eta$), and Net ($\delta F_N/\Delta\eta$) Sensitivity Factors for July

Latitude	Solar (1200 LT)	IR (1200 LT)	Net (1200 LT)	Net (Average Daily)
2.25	237.3	−65.3	−172.1	−25.9
6.75	298.8	−85.0	−213.8	−44.0
11.25	223.2	−74.0	−149.2	−25.6
15.75	192.2	−72.0	−120.2	−16.8
20.25	144.3	−54.9	−89.5	−13.2
24.75	160.3	−55.3	−104.8	−25.9
29.25	217.8	−72.1	−145.7	−36.7
33.75	262.1	−79.8	−182.3	−52.2
38.25	300.1	−84.7	−216.0	−78.6
42.75	303.9	−81.9	−221.9	−70.4
47.25	318.6	−77.7	−240.8	−77.5
51.75	342.0	−74.1	−267.9	−70.1
56.25	368.2	−73.1	−295.3	−87.4
60.75	378.2	−80.6	−297.6	−113.4
65.25	289.8	−64.4	−225.4	−110.9
69.75	140.0	−36.5	−103.5	−104.3
74.25	81.5	−25.5	−56.1	−63.7
78.75	52.4	−23.1	−29.5	−39.3
83.25	29.6	−22.8	−6.8	−7.1
87.75	6.0	−20.3	14.3	14.2
Northern hemisphere	245.1	−69.3	−175.7	−50.9

Sensitivity factors are stated in units of watts per square meter/percent.

4.3. *Northern Hemisphere Cloud/Radiation Sensitivity*

The values of the 1200 LT solar, IR, and net radiation sensitivity factors and the 1200 LT IR/albedo sensitivity factor for each TA are obtained from the slope of the least squares linear regression line associated with the scatter diagrams of the 1200 LT radiation parameters and cloud amounts or albedos. For presentation purposes, only the net radiation and IR/albedo sensitivity results are illustrated in Figure 11 for January and Figure 12 for July.

In January the region of low total cloud amounts for the Afro-Asian desert is characterized by low IR, solar, net, and IR/albedo sensitivity values. These low values can be attributed to the small surface–cloud top temperature differences and the small surface-cloud albedo differences. As indicated earlier, low IR/albedo sensitivity values usually imply large net radiation sensitivity factors. The exception to this rule occurs for regions where the surface cloud albedo difference is small. Regions of high albedos are usually associated with deserts or snow-covered ground.

The United States east coast storm track is characterized by high IR and solar sensitivity values. These high values are a result of considerable variation in the surface-cloud albedo difference and the surface–cloud top temperature difference, which is characteristic of the multilayered cloud structure associated with the storms in this region. The northern United States west of the Great Lakes and most of Canada west of the Hudson Bay have sensitivity values similar to those associated with the Afro-Asian desert. In this region the high surface albedo is due to the extensive snow cover. The IR sensitivity values associated with the region off the west coast of the

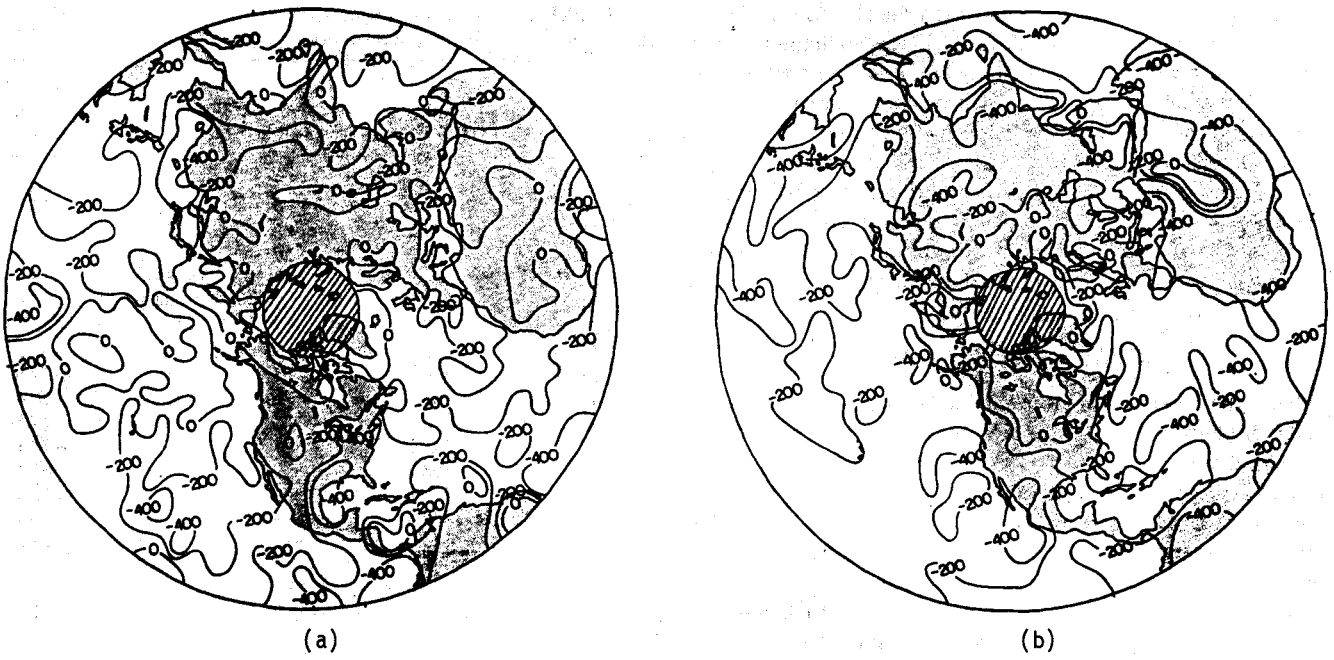

Fig. 11. The northern hemisphere 1200 LT sensitivity factors (*a*) $\Delta F_N/\Delta\eta$ and (*b*) $\Delta F_{IR}/\Delta r$ for January 1979.

United States are much greater in January than in July. This change in the values from July to January reflects a change in the cloud types associated with this region. The predominant cloud type in July is stratus. In January the high frequency of storms moving through this area results in more convective type clouds. For July the surface–cloud top temperature difference is small and there is very little variation in this difference, while in January the surface–cloud top temperature difference is greater, as is the variation of this difference. The values of the sensitivity factors for eastern China and the East and South China seas clearly indicate that the predominant cloud type is stratus.

In July, Africa is extremely interesting because of the large variability of the total cloud amounts and the surface albedos. The desert areas are characterized by high surface albedos and low total cloud amounts. The corresponding solar, IR, and IR/albedo sensitivity values are low, while the net radiation sensitivity value is positive, indicating that the albedo effect of the clouds is less than the greenhouse effect. Equatorial Africa has low surface albedos and high cloud amounts. This region is associated with the ITCZ, which is characterized by a high frequency of convective activity. For this region an increase in the cloud amount decreases the net radiation.

The major circulation features are very evident on the sensi-

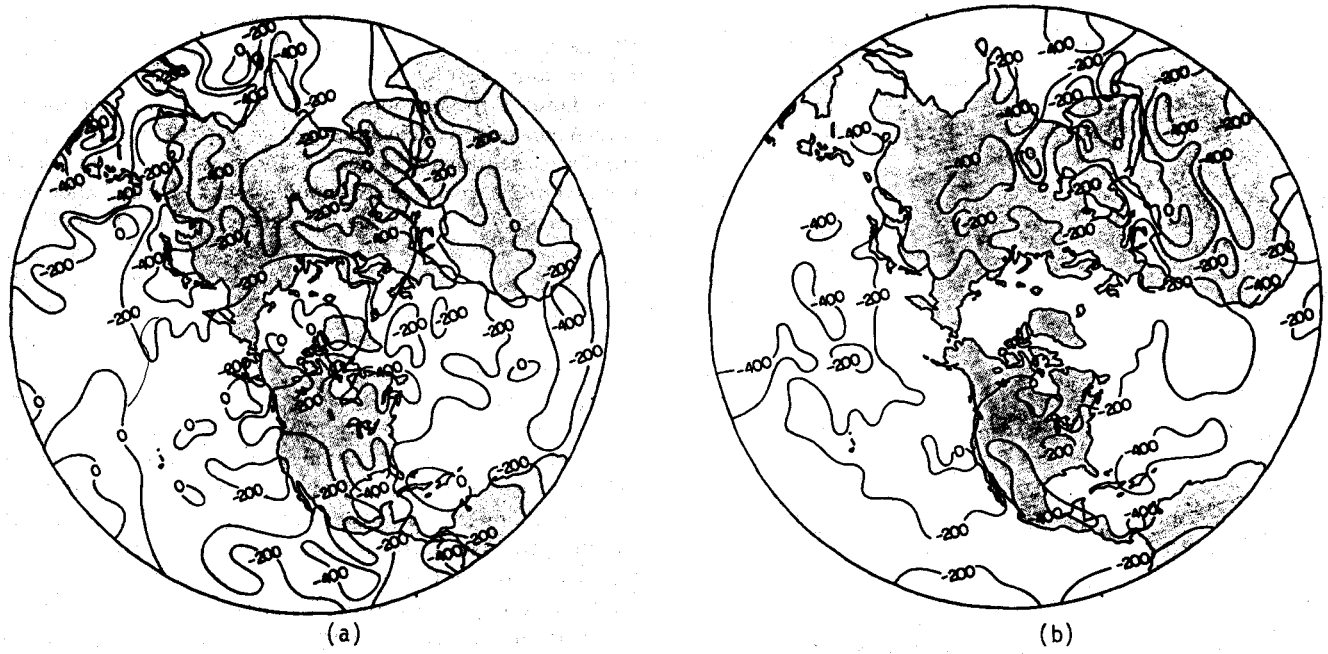

Fig. 12. The northern hemisphere 1200 LT sensitivity factors (*a*) $\Delta F_N/\Delta\eta$ and (*b*) $\Delta F_{IR}/\Delta r$ for July 1979.

tivity maps. The tropical and subtropical highs correspond to regions of low IR, solar, and net radiation sensitivity values. The ITCZ in the eastern Atlantic, western and eastern Pacific, and in the region of the monsoon are characterized by high solar and IR sensitivity values. The high net radiation sensitivity factors in the tropical areas of the eastern Atlantic and western Pacific are not consistent with the high value of the IR/albedo sensitivity factor. In the eastern Pacific ITCZ region, the net radiation sensitivity factor exhibits considerable spatial variability, which is characteristic of a region composed of both stratus and convective clouds. The stratus off the west coast of the United States is well defined by the high solar and net radiation sensitivity factors and the corresponding low IR sensitivity values.

The January 1200 LT values of the solar, IR, and net radiation sensitivity factors for the northern hemisphere are 191.9, −57.5, and 134.4 W m^{-2}, respectively, while the values for July are 245.1, −69.3, and −175.7 W m^{-2}. The regional, zonal and global values of the net radiation sensitivity factor indicate that the albedo effect of clouds is greater than the greenhouse effect for almost all regions of the northern hemisphere. The greenhouse effect is greater than the albedo effect only in regions where the surface-cloud albedo difference is small and for the polar regions of the wintertime hemisphere.

5. SUMMARY

Northern hemisphere monthly mean cloud and ERB climatologies have been developed for January and July 1979 from the AFGWC 3DNEPH cloud analysis and the Nimbus 7 ERB STRTs, respectively. The cloud climatologies are consistent with the zonal and global general circulation features. The zonal cloud climatologies for January and July clearly indicate the position of the tropical and subtropical highs, and the ITCZ and mid-latitude depression, and the northward movement of these features during the summer. The 3DNEPH zonal cloud climatologies compare favorably with existing climatologies, with the following exceptions: the Arctic wintertime cloud climatology is not reliable, and the summertime ITCZ cloud amounts appear to be overestimated. The latter problem may be due to incorrect DMSP tuning factors, which, according to the AFGWC 3DNEPH quality control log, were corrected in August 1979. Also, it is noted that the 3DNEPH climatology underestimates the high cloud amounts, especially in the tropics, and overestimates the thickness of the middle clouds.

The global cloud distributions are consistent with the global outgoing solar and IR flux distributions. In the tropics the large zonal variations of the solar and IR fluxes are consistent with the longitudinal variations in the cloud amounts. These zonal variations in the fluxes, which are of the same order of magnitude as the meridional variation, have been well documented in the literature. In addition, the outgoing IR fluxes at the top of the atmosphere, obtained from the University of Utah parameterization model using the zonal 3DNEPH layered cloud climatologies and the atmospheric statistics of *Oort and Rasmusson* [1971], are in close agreement with the ERB zonal fluxes.

Using the 3DNEPH cloud and ERB data bases for January and July 1979, a number of cloud/radiation sensitivity factors are investigated. These factors include the changes in solar, IR, and net fluxes derived from ERB data, with respect to the change in cloud cover determined from 3DNEPH cloud data. On a regional basis the solar albedo effects prevail over most of the regions selected for this study, except over deserts and snow fields. The predominance of the solar albedo effect is also evident from the zonally averaged sensitivity factors for the northern hemisphere. Except for a few northern latitudinal zones for January, the sensitivity of the net flux change due to the cloud cover variation is controlled by the reflected solar flux. The average global, IR, and net radiation sensitivity values computed using the actual cloud amounts are close to the values determined indirectly by *Hartmann and Short* [1980] and *Ohring et al.* [1981], even though the satellites involved in these investigations have different equator-crossing times and spectral intervals.

Acknowledgments. This research was supported in part by the Air Force Geophysics Laboratory under contract F19628-84-K-0040. We thank Roy Jenne and Dennis Joseph of the National Center for Atmospheric Research for their assistance in providing the necessary computer time to process the 3DNEPH and ERB data sets. Sharon Bennett typed and edited the manuscript.

REFERENCES

Arking, A., and S. Vemury, The Nimbus 7 ERB data set: A critical analysis, *J. Geophys. Res.*, *89*, 5089–5097, 1984.

Berlyand, T. G., and L. A. Strokina, Global distribution of total cloud amount, *Gidrometeoizdata*, Leningrad, translated from Russian by S. Warren, 18 pp., 1980.

Brooks, C. E. P., The mean cloudiness over the earth, *Mem. R. Meteorol. Soc.*, *1*, 127–138, 1927.

Cess, R. D., Climate change: An appraisal of atmospheric feedback mechanisms employing zonal climatology, *J. Atmos. Sci.*, *33*, 1831–1843, 1976.

Cess, R. D., B. P. Briegleb, and M. S. Lian, Low-latitude cloud amount and climate feedback: Comparative estimates from satellite data, *J. Atmos. Sci.*, *39*, 53–59, 1982.

Environmental Technical Applications Center, Northern hemisphere cloud cover, ETAC project 6168, 20 pp., U.S. Air Force, Washington, D.C., 1971.

Gordon, C. T., R. D. Hovanec, and W. F. Stern, Analysis of monthly mean cloudiness and their influence upon model diagnosed radiative fluxes, *J. Geophys. Res.*, *89*, 4713–4738, 1984.

Hartmann, D. L., and D. A. Short, On the use of earth radiation budget statistics for studies of clouds and climate, *J. Atmos. Sci.*, *37*, 1233–1250, 1980.

Heymsfield, A. J., and C. M. R. Platt, Parameterization of the particle size spectrum of ice clouds in terms of ambient temperature and ice water content, *J. Atmos. Sci.*, *41*, 846–855, 1984.

Hughes, N. A., Global cloud climatologies: A historical review, *J. Clim. Appl. Meteorol.*, *23*, 724–751, 1984.

Jacobowitz, H., L. L. Stowe, and J. R. Hickey, The Earth Radiation Budget (ERB) Experiment, the Nimbus 7 User's Guide, pp. 33–69, NASA Goddard Space Flight Center, Greenbelt, Md., 1978.

Jacobowitz, H., H. V. Soule, H. L. Kyle, F. House, and the Nimbus 7 Experiment Team, The earth radiation budget (ERB) experiment: An overview, *J. Geophys. Res.*, *89*, 5021–5038, 1984.

Koenig, G. G., Cloud and radiation budget studies, Ph.D. Dissertation, 308 pp., Univ. of Utah, Salt Lake City, 1984.

Liou, K. N., and S. C. Ou, Parameterization of infrared radiative transfer in cloudy atmospheres, *J. Atmos. Sci.*, *38*, 2707–2716, 1981.

Liou, K. N., and G. D. Wittman, Parameterization of infrared radiative transfer in cloudy atmospheres, *J. Atmos. Sci.*, *36*, 1261–1273, 1979.

London, J., A study of the atmospheric heat balance, final report, contract AF19(122)-165 (AFCRC-TR-57-287), 99 pp., New York Univ., New York, 1957.

Miller, D. B., and R. G. Feddes, Global atlas of relative cloud cover, *AD739434*, *Rep. 1*, 14 pp. and charts, U.S. Nat. Environ. Satell. Serv. and U.S. Air Force Environ. Tech. Appl. Cent., Washington, D.C., 1971.

Müller, M. J., *Selected Climatic Data for a Global Set of Standard Stations for Vegetation Science*, 306 pp., W. Junk, Boston, 1982.

Ohring, G., and P. F. Clapp, The effect of changes in cloud amount on the net radiation at the top of the atmosphere, *J. Atmos. Sci.*, *37*, 447–454, 1980.

Ohring, G., P. F. Clapp, T. R. Heddingaus, and A. F. Krueger, The quasi-global distribution of the sensitivity of the earth-atmosphere radiation budget to clouds, *J. Atmos. Sci.*, *38*, 2539–2541, 1981.

Oort, A. H., and E. M. Rasmusson, Atmospheric Circulation Statistics, *NOAA Prof. Pap. 5*, 323 pp., Natl. Oceanic and Atmos. Admin., Boulder, Colo., 1971.

Ou, S. C., and K. N. Liou, Parameterization of carbon dioxide 15 μm absorption and emission, *J. Geophys. Res.*, *88*, 5203–5207, 1983.

Schneider, S. H., Cloudiness as a global climatic feedback mechanism: The effect on the radiation balance and surface temperature of variations in cloudiness, *J. Atmos. Sci.*, *29*, 1413–1422, 1972.

Schutz, C., and W. L. Gates, Global climate data for surface, 800 mb and 40 mb: January, *Rep. R-915-ARPA*, 21 pp., Rand Corporation, Santa Monica, Calif., 1971.

Taylor, V. R., and L. L. Stowe, Reflectance characteristics of uniform earth and cloud surfaces derived from Nimbus 7 ERB, *J. Geophys. Res.*, *89*, 4987–4996, 1984.

Taylor, V. R., L. L. Stowe, and J. M. Vilardo, Nimbus 7 ERB reflectance models for ERBE processing, *Conf. Atmos. Radiat., Prepr., 5th*, 452–455, 1983*a*.

Taylor, V. R., J. M. Vilardo, L. L. Stowe, and S. K. Vemury, 1983*b*: Nimbus 7 ERB emission models for ERBE processing, *Conf. Atmos. Radiat., Prepr., 5th*, 433–435, 1983*b*.

M. Griffin and K.-N. Liou, Department of Meteorology, University of Utah, Salt Lake City, UT 84112.

G. Koenig, Air Force Geophysics Laboratory, Hanscom Air Force Base, Bedford, MA 01731.

(Received December 31, 1985;
revised February 9, 1987;
accepted February 11, 1987.)